Modified hyper-viscoelastic damage evolution constitutive model for polyurethane materials–an experimental and numerical investigation

Modified Hyper-viscoelastic Damage Evolution Constitutive Model for Polyurethane Materials - An Experimental and Numerical Investigation

Mina Jahanmardi[1], Hossein Hosseini-Toudeshky[1*], Mohammad Saeed Goodarzi[2], Erasmo Carrera[3], Alfonso Pagani[3]

[1]*Department of Aerospace Engineering, Amirkair University of Technology, Iran*

[2]*Department of Industrial, Mechanical and Aerospace Engineering, Buein Zahra Technical University, Qazvin, Iran*

[3]*Deparment of Mechanical and Aerospace Engineering, Polytechnic University of Turin, Turin, Italy*

Abstract

Elastomeric materials are widely used in different industries due to their excellent capability to withstand different loading types. There are significant challenges to the efficient design of elastomeric structures because of the rate-dependent and highly nonlinear behavior of this type of material. In the present study, a damage zone model was employed to simulate the material behavior and damage evolution in polyurethane elastomers with different shore hardness. This model consists of three sections, hyper viscoelastic constitutive model, damage initiation and damage evolution using a hyper viscoelastic traction-separation law. To simulate the nonlinear behavior of polyurethane, a rate-dependent factor implemented into the Mooney-Rivlin strain density function with 9 parameters. The material characteristics are specified by performing the experimental tests for 3 different shore hardness. In the present study, a user-defined subroutine (VUMAT) was developed to predict the damage evolution in the pure shear tearing specimen of polyurethane elastomers. The results verification proves a good agreement between the FEA simulation and experimental data. Therefore, the developed numerical analysis procedure can be used to investigate the damage initiation and evolution in elastomeric materials.

Introduction

Elastomeric polymer composites are used in a wide variety of engineering structures. Investigations clearly show that elastomers have a significant contribution in increasing and strengthening the protective performance of elastomeric polymer composites. The effective factor in this performance is exceptional mechanical and thermal properties along with the property of automatic recovery. The elastomeric polymer coating also improves the

deformability of composite structures, as a result of which the energy absorption capacity increases impressively. Polyurethane (PU) is the most widely used elastomer in the industry, which behaves both hyperplastic and viscoelastic. PU is the result of the chemical reaction of polyol and isocyanates. Recently, some investigations worked on the combination of elastomeric polyurethane with carbon fibers to make a more eco-friendly and stronger composite materials [1]. The nonlinear behavior of elastomers involves significant challenges in modeling and investigating the performance of these materials under dynamic loading. This nonlinear behavior caused by the long-chain molecular structure leads to hyper-viscoelastic properties of the elastomers. Another interesting feature is that the mechanical properties of elastomers are not only affected by pressure and temperature, but also by changing the loading rate. All elastomer products possess microscopic defects which are the basis of the damage initiation in these materials. These microscopic flaws colligate together to shape a crack and growth during the time under loading. Therefore, investigations on prediction of crack initiation and evolution in elastomers seems to be a crucial issue. However, most of the previous studies on the mechanics of elastomeric material worked on the description of material behavior and deformations, and there is a limited number of investigations focused on the damaged modeling. Gurvich [2] proposed a general methodology for behavioral modeling and fracture investigation in adhesive element-based hyperelastic materials, focusing specifically on nonlinear hyperelastic problems. In this research paper a cohesive element-based modeling was developed containing three steps of determining possible locations for the onset of crack damage and orientation of expected cracks. All modeling and analyses features were selected to achieve an almost accurate response and the hyperplastic deformation was defined by the Hookean-Neo law. The major damage mechanisms were considered independently and the initial gap in the middle of the specimen was expected to be under uniaxial stress. Nair et al. [3] also utilized standard test data to model multiaxial loading modes, fracture of hyperelastic materials, simulation of indentation test, and then determined the failure characteristics of hyperelastic materials using finite element method. The failure model based on the adhesive area has been used to simulate the crack growth in Abacus software, and also the two-line stretch-separation model used to simulate the onset and crack growth in the rupture test. Elmukashfi et al. [4] analyzed the expansion of dynamic cracks in the elastic region. In this research, the growth of dynamic cracks in the elastic region has been analyzed numerically using the finite element method. The performed FEA was non-linear and

implicit. Also, the behavior of materials was defined based on the viscoelastic theory and the characteristics of the separation process using the adhesive region model with the bilinear traction separation law. Following that, the adhesive region theory used for numerical analysis of failure and the Maxwell model was used to calculate the total strain energy, which also includes the viscous response. Venkata [5] simulated the butadiene styrene elastic rupture using finite element analysis focused on the onset and spread of failure in styrene butadiene elastic (SBR) plates. In his research, using the concept of adhesive zone at the crack tip, a special traction-separation law was proposed in the elastic structural equations and then the hyper-viscoelastic fracture equations were implemented in a VUMAT subroutine in Abaqus software. Therefore, the failure of SBR plates under dynamic tensile loading has been predicted. In another study, Lev and et al [6] modeled the growth and expansion of cracks in the elastic region. This simulation has been performed by the dynamic version of DYNA-LS limited element software. By implementing the user defined subroutines, simulation of an elastic plate cracking stretched in two directions was performed. Volokh [7] has investigated the approach of energy limiters to model elastic fracture. In this research, the examination of the new approach of energy limiters along with hyperelastic theories made it possible to see the failure process. Based on this approach, the onset of failure has been predicted but its propagation was not traced. Finally, the theory is used to numerically simulate the three-dimensional high-velocity penetration of a rigid elastic object into an elastic plane. The failure of elastomers due to cavitation has been also investigated by Hamdi et al. [8]. They studied the phenomenon of cavitation in quasi-elastic materials, with a combination of experimental, theoretical and numerical approaches, and designed and performed special experiments on styrene-butadiene elastic in order to show the main properties of cavitation. This investigation showed that the hydrostatic critical pressure and the overall critical deformation control the formation of the cavitation nucleus. Conventional hyperelastic models cause the accumulation of strain energy indefinitely. The phenomenon of accumulation is non-physical and the possibility of material failure should be considered in the description of the model theory. Implementing energy limiters in strain energy formulation is a proper way to describe the failure. Li et al. [9], proposed an adhesive zone model to predict dynamic rupture in the rubberlike materials. The aim of this work was to develop a numerical model according to adhesive zone theory to investigate the growth of cracks in tires under tearing loading. The extended numerical model was attached to Abaqus software to simulate the

adhesive region. The adhesive zone model was used to predict the crack growth in hyperelastic materials based on the idea of energy release rate first developed by Griffith [10]. Rivlin and Thomas [11] then developed a criterion for tearing of rubber based on Griffith's energy perspective. Being independent from the shape of the test specimen is the main advantages of using this method which leads to better find the mechanical properties affecting the tearing of a test specimen. In most of the previous researches, in order to model the hyper viscoelastic behavior of elastomer materials, the Maxwell rheological model was used to derive the total Cauchy stress coming from both hyperelastic and viscoelastic material properties.

In the current investigation, using the hyper viscoelastic strain density potential provided by Somarathna et al. [12] the behavior of PU elastomers is modeled which lead to more accurate results while reducing the modeling complications. In addition, the damage initiation and evolution are employed according to the cohesive zone modeling approach. The cohesive hyperviscoelastic traction-separation law is also used a user defined material subroutine in the commercial finite element software for damage modeling of PU material with different shore hardness. The material characteristics are specified by performing the experimental tests for 3 different shore hardness. The predicted results are verified with experimental results.

1. Hyper-Viscoelastic Damage Model

In this research, the damage constitutive law based on the traction-separation curve shown in Fig. 1 was developed as a VUMAT subroutine to predict the damage initiation and evolution in the polyurethane material. During the crack growth in elastomers, there exists a damage zone ahead of the crack tip. The material behavior in this zone can be modeled based on the cohesive zone modeling approach in terms of an equivalent traction-separation law proposed by Li [8]. This traction-separation law consists of three events as shown in Fig. 1. The line OA is representative of the hyper viscoelastic behavior of the elastomer before damage, point A is relevant with damage initiation and line AB is representative of the behavior of the material after damage initiation concurrent with the stiffness degradation. In this model, T is denoted by the equivalent stress and δ is denoted by the equivalent strain.

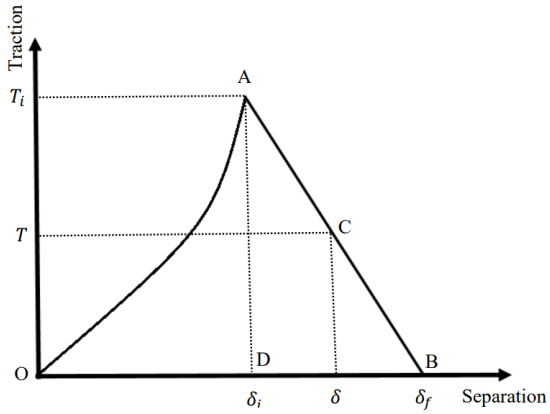

Fig.1. Traction-separation law used in damage zone model

The hyper viscoelastic behavior, OA, is developed using a hyper viscoelastic strain density function. As a matter of fact, elastomeric material behavior is crucially dependent on strength and energy absorption in the application of dynamic forces. Since hyperelastic strain density is independent of strain rate, it is necessary to consider strain rate-dependent functions in conjunction with genuine hyperelastic strain density function so that a constitution law can be developed to precisely predict the material behavior. The current study is devoted to simulating hyper-viscoelastic behavior establishing the dynamic increase factor proposed by Somarathna et al. [12] into the Mooney-Rivlin strain density function to make a hyper-viscoelastic strain density function. In previous researches, the Mooney-Rivlin strain density function with 9 parameters was introduced to have more accurate results in predicting elastomeric materials' nonlinear behavior.

$$\psi(I_1, I_2, \mathrm{J}) = C_{10}(\bar{I}_1 - 3) + C_{01}(\bar{I}_2 - 3) + C_{11}(\bar{I}_1 - 3)(\bar{I}_2 - 3) + C_{20}(\bar{I}_1 - 3)^2 + \quad (1)$$
$$C_{02}(\bar{I}_2 - 3)^2 + C_{21}(\bar{I}_1 - 3)^2(\bar{I}_2 - 3) + C_{12}(\bar{I}_1 - 3)(\bar{I}_2 - 3)^2 + C_{30}(\bar{I}_1 - 3)^3 + C_{03}(\bar{I}_2 - 3)^3 + D_1(J - 1)^2$$

Where, ψ is the Mooney-Rivlin strain density function, C_{10}, C_{01}, C_{11}, C_{20}, C_{02}, C_{21}, C_{12}, C_{12}, C_{30}, C_{03} and D_1 are the material constants determined by the experimental tests, $\bar{I}_1$ and $\bar{I}_2$ are the first and second invariants of the left Cauchy deformation tensor respectively and J is the determinant of deformation gradient tensor. In this study, it has assumed that the material behavior is nearly incompressible (J=det(**F**)=1). The strain density function used in this study is the hyper viscoelastic Mooney-Rivlin strain density potential [12].

$$W = \Psi(I_1, I_2)(1 + \frac{1}{A}(ln\dot{\epsilon}^*)^N) \quad (2)$$

A and N are calculated from the experimental tests and they are the coefficients of dynamic increase factor (DIF) which is multiplied by the conventional strain density function as the rate-dependent parameter.

$$\text{DIF}=(1 + \frac{1}{A}(ln\dot{\epsilon}^*)^N) \quad (3)$$

$\dot{\epsilon}^*$, the normalized strain rate, is specified as the ratio of the actual strain rate to the reference strain rate. Based on the theory of the hyperplastic material, the stress can be calculated as:

$$\sigma = (2[(\Psi_1 + I_1\Psi_2)B - \Psi_2 B.B] - \text{pI})) \ (1 + \frac{1}{A}(ln\dot{\epsilon}^*)^N) \quad (4)$$

Where,

$\Psi_1 = \frac{\partial \psi}{\partial I_1}$, $\Psi_2 = \frac{\partial \psi}{\partial I_2}$, B=FF^T and p is the hydrostatic pressure. (5)

1.2 Damage evolution model

The material behavior is simulated based on the hyper viscoelastic constitutive model. As soon as the damage initiates (point A in Fig.1), the material properties and consequently the material stiffness are degraded. To describe the stiffness degradation, a damage parameter is defined based on the traction-separation law which is representative of the damage evolution in the material.

2.2.1 Damage initiation

Point A in Fig. 1 is the damage initiation point. Many researches indicated that necking or local thinning leads the crack to develop in the elastomers. Based on these observations, it is considered that there is a critical negative pressure at which all the cavities inside the elastomer will burst. Therefore, the critical hydrostatic tensile pressure (p_{cr}) obtaining from experimental results, can be assumed as the fracture criterion for thin elastomers [9]. In other words, damage initiates when the hydrostatic pressure meets the critical value.

$$p \geq p_{cr} \quad (6)$$

$$p = \frac{1}{3}(\sigma_{xx} + \sigma_{yy} + \sigma_{zz}) \quad (7)$$

Where p is the hydrostatic pressure, and σ_{xx}, σ_{yy} , and σ_{zz} are the normal stresses and for the uniaxial tension loading along the x axis, σ_{yy} and σ_{zz} are equal to zero. Based on the rate dependent behavior of the elastomeric materials, the hydrostatic tensile pressure is rate-dependent as well. Therefore in the present study, the hydrostatic tensile pressure is assumed as follows:

$$p = \frac{1}{3}(\sigma_{xx} + \sigma_{yy} + \sigma_{zz})\ (1 + \frac{1}{A}(ln\dot{\epsilon}^{*})^{N}) \tag{8}$$

2.2.2 Damage Evolution

Once the damage initiation is occurred, the degradation of material properties is started. Based on the equivalent traction-separation law, the degradation path AB in Fig. 1 can be expressed as a linear damage evolution criterion as follows:

$$T = T_i\left(\frac{\delta_f - \delta}{\delta_f - \delta_i}\right) \tag{9}$$

In this study, it has been considered that only the tensile components of strain cause damage. Therefore, considering I_1 to be the first invariant of the left Cauchy deformation tensor, in the case that p is equal to p_{cr}, the equivalent stretch ratio ($\bar{\lambda}$) for the incompressible elastomer is defined as [9]:

$$I_1 = \bar{\lambda}^2 + \frac{2}{\bar{\lambda}} \tag{10}$$

Therefore the equivalent stretch ratio is determined by calculating the largest positive root of the following equation:

$$\bar{\lambda}^3 - I_1\bar{\lambda} + 2=0 \tag{11}$$

As a result the equivalent stress T in the traction-separation law is given by:

$$T = 2\,C_{10}\Bigg\{\Bigg(1+\alpha_1\left(\lambda^2+\frac{2}{\lambda}-3\right)+2\alpha_4\left(2\lambda+\frac{1}{\lambda^2}-3\right)+\alpha_5\left(\lambda^2+\frac{2}{\lambda}-3\right)^2+\alpha_6\left(\lambda^2+\frac{2}{\lambda}-3\right)+3\alpha_8\left(2\lambda+\frac{1}{\lambda^2}-3\right)^2\Bigg)\left(\lambda^4-\frac{1}{\lambda^2}\right)+\Bigg(\Bigg(1+\alpha_2\left(2\lambda+\frac{1}{\lambda^2}-3\right)+2\alpha_3\left(\lambda^2+\frac{2}{\lambda}-3\right)+2\alpha_5\left(\lambda^2+\frac{2}{\lambda}-3\right)\left(2+\frac{1}{\lambda^2}-3\right)+\alpha_6\left(2\lambda+\frac{1}{\lambda^2}-3\right)+3\alpha_7\left(\lambda^2+\frac{2}{\lambda}-3\right)^2\Bigg)+\alpha_1\left(\lambda^2+\frac{2}{\lambda}\right)+\alpha_2\left(\lambda^2+\frac{2}{\lambda}\right)\left(\lambda^2+\frac{2}{\lambda}-3\right)+2\alpha_4\left(\lambda^2+\frac{2}{\lambda}\right)\left(2\lambda+\frac{1}{\lambda^2}-3\right)+\alpha_5\left(\lambda^2+\frac{2}{\lambda}\right)\left(\lambda^2+\frac{2}{\lambda}-3\right)^2+\alpha_6\left(\lambda^2+\frac{2}{\lambda}\right)\left(\lambda^2+\frac{2}{\lambda}-3\right)+3\alpha_8\left(\lambda^2+\frac{2}{\lambda}\right)\left(2\lambda+\frac{1}{\lambda^2}-3\right)^2\Bigg)\left(\frac{1}{\lambda}-\lambda^2\right)\Bigg\}\left(1+\frac{1}{A}(ln\dot{\epsilon}^*)^N\right) \tag{12}$$

In this equation, α_1 to α_8 are the ratios of the Mooney-Rivlin coefficients which are assumed to be constant before and after damage initiation.

$$\alpha_1=\frac{C_{01}}{C_{10}},\ \alpha_2=\frac{C_{11}}{C_{10}},\ \alpha_3=\frac{C_{20}}{C_{10}},\ \alpha_4=\frac{C_{02}}{C_{10}},\ \alpha_5=\frac{C_{21}}{C_{10}},\ \alpha_6=\frac{C_{12}}{C_{10}},\ \alpha_7=\frac{C_{30}}{C_{10}},\ \alpha_8=\frac{C_{03}}{C_{10}} \tag{14}$$

Based on (9), describing the damage evolution as a linear function and equating the right hand side of (9) and (12), gives:

$$C_{10d}=\frac{T_i\left(\frac{\delta_f-\delta}{\delta_f-\delta_i}\right)}{2\left\{\begin{matrix}\left(1+\alpha_1\left(\lambda^2+\frac{2}{\lambda}-3\right)+2\alpha_4\left(2\lambda+\frac{1}{\lambda^2}-3\right)+\alpha_5\left(\lambda^2+\frac{2}{\lambda}-3\right)^2+\alpha_6\left(\lambda^2+\frac{2}{\lambda}-3\right)+3\alpha_8\left(2\lambda+\frac{1}{\lambda^2}-3\right)^2\right)\left(\lambda^4-\frac{1}{\lambda^2}\right)+\\ \left(\begin{matrix}\left(1+\alpha_2\left(2\lambda+\frac{1}{\lambda^2}-3\right)+2\alpha_3\left(\lambda^2+\frac{2}{\lambda}-3\right)+2\alpha_5\left(\lambda^2+\frac{2}{\lambda}-3\right)\left(2+\frac{1}{\lambda^2}-3\right)+\right)+\\ \alpha_6\left(2\lambda+\frac{1}{\lambda^2}-3\right)+3\alpha_7\left(\lambda^2+\frac{2}{\lambda}-3\right)^2\end{matrix}\right)+\\ \alpha_1\left(\lambda^2+\frac{2}{\lambda}\right)+\alpha_2\left(\lambda^2+\frac{2}{\lambda}\right)\left(\lambda^2+\frac{2}{\lambda}-3\right)+\\ 2\alpha_4\left(\lambda^2+\frac{2}{\lambda}\right)\left(2\lambda+\frac{1}{\lambda^2}-3\right)+\alpha_5\left(\lambda^2+\frac{2}{\lambda}\right)\left(\lambda^2+\frac{2}{\lambda}-3\right)^2+\alpha_6\left(\lambda^2+\frac{2}{\lambda}\right)\left(\lambda^2+\frac{2}{\lambda}-3\right)+3\alpha_8\left(\lambda^2+\frac{2}{\lambda}\right)\left(2\lambda+\frac{1}{\lambda^2}-3\right)^2\end{matrix}\right)\left(\frac{1}{\lambda}-\lambda^2\right)\Bigg\}\left(1+\frac{1}{A}(ln\dot{\epsilon}^*)^N\right)}$$

Where, c_{10d} is the damaged parameter of Mooney-Rivlin function. T_i and δ_i are the equivalent stress and displacement at damage initiation which are calculated by the critical tensile pressure and δ_f is the final equivalent displacement which is calculated based on the tearing energy of the elastomer. The area under the traction-separation diagram is equal to the total tearing energy G. Considering the areas under OAD and ADB in Fig. 1 as G_1 and G_2 respectively, it will be concluded that,

$$G_2 = G - G_1 \tag{15}$$

On the other hand the amount of G_2 can be derived from the traction-separation curve as:

$$G_2 = \frac{1}{2} T_i (\delta_f - \delta_i) \tag{16}$$

By equating the (15) and (16), the equivalent final displacement can be calculated as:

$$\delta_f = \delta_i + \frac{2(G - G_1)}{T_i} \tag{17}$$

In the present study, the total tearing energy G, is calculated based on the experimental results and the calculation of G_1 will be explained in the next sections. The procedure of the damage analyses for Polyurethane elastomers is illustrated in Fig. 2.

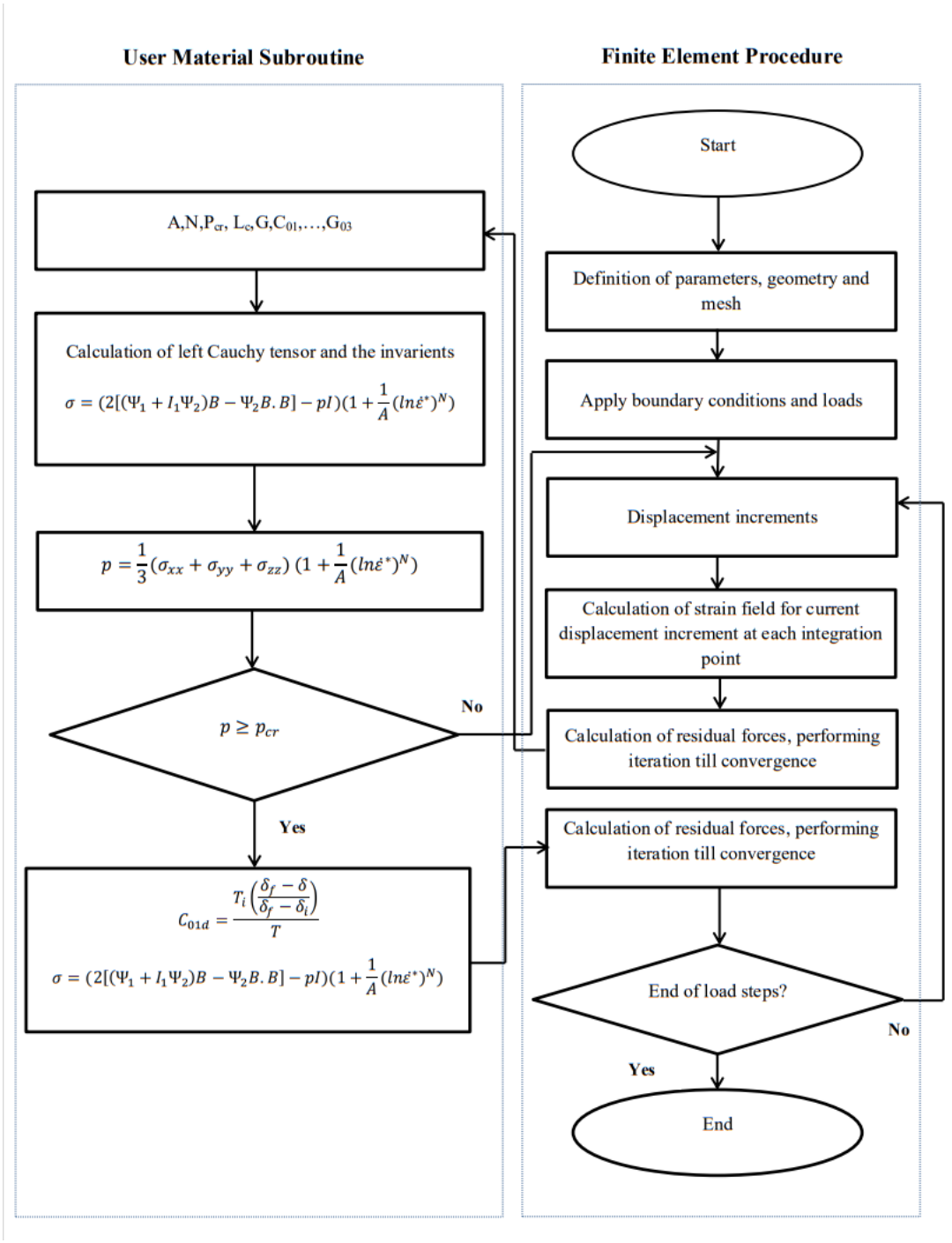

Fig 2. Procedure of the progressive damage analyses for Polyurethane elastomers

2. Material Characterization

In most of the previous researches the conventional strain density is used to simulate the highly nonlinear behavior of elastomers. Currently, researchers has focused on the high strain rate dependency of the elastomers to model both hyperelastic and viscoelastic behaviors. In this study, Mooney-Rivlin strain density function with 9 parameters is multiplied by the dynamic increase factor (DIF) proposed by Somarathna et al. [12] to simulate the hyper viscoelastic behavior of Polyurethane under different strain rates.

To calculate the 9 parameters of Mooney-Rivlin strain density function and 2 parameters of dynamic increase factor (DIF), the uniaxial tension loading test has been performed under different strain rate from 0.001 s^{-1} to 0.33 s^{-1}. In addition, as it is discussed in the previous section the critical tearing energy of the elastomer (G) should be calculated from experiments. These tests were performed using pure shear specimens with strain rate of 0.33 s^{-1}. The specimens provided for the experiments were polyurethane elastomer with 3 different shore hardness of 60, 75 and 85. These shore hardness are in the group of shore-A.

2.1 Uniaxial Tension Tests

The uniaxial tension loadings were accomplished under different strain rate from 0.001 s^{-1} to 0.33 s^{-1} to calculate the DIF and Mooney-Rivlin coefficients [14]. These experiments followed the procedure described in the ASTM D-412 standard. The stress-strain curves plotted under the assumption that the polyurethane is nearly incompressible. Afterwards the above mentioned coefficients were calculated by curve fitting method. More details of the procedure has been described in our previous study, from which the coefficients summarized in Table 1 [14].

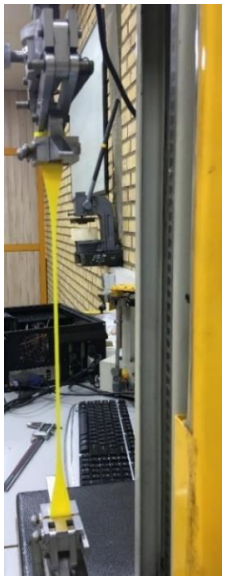

Fig 3. Uniaxial tension loading test [14]

Table 1. Parameters of Mooney-Rivlin strain density potential under the strain rate of 0.33 s^{-1} and the coefficients of DIF for shore hardness of (a) 60, (b) 75, and (c) 85 [14]

(a)

C01	C10	C20	C11	C02	C30	C21	C12	C03	A	N
45.6288	-45.5725	0.69619	-0.69619	-0.298257	-19.6106	0.0437261	-0.410836	-0.910154	2.33	1.61

(b)

C01	C10	C20	C11	C02	C30	C21	C12	C03	A	N
38.3439	-38.3411	0.6691	-0.577837	-15.3614	0.0351788	-0.352602	0.906826	-0.54934	4.35	2.014

(c)

C01	C10	C20	C11	C02	C30	C21	C12	C03	A	N
154.78	-154.056	-6.27553	-1.82423	82.8168	0.448776	--0.638023	-3.07212	-6.44244	5.8	3.02

2.2 Tearing energy

The tearing energy in elastomeric materials is representative of the fracture toughness property. Modification of Griffith's approach to the tearing performance of rubbers by Rivlin and Thomas [11, 15] became the basis for defining the tearing energy as a crack growth criterion in rubberlike materials. Then, Lake et al. verified this approach by performing several investigations and proved that the damage growth is independent of geometry [16-19]. There are three common test specimens for evaluation of the elastomer fracture depends on the loading mode and deformation rate of the experiments. In this study, the pure shear specimen is employed. The specimen is a wide strip of elastomer material with dimensions shown in Fig.4, connected to rigid grips of the testing machine from its long edge as shown in Fig. 5 and subjected to a uniform strain rate of 0.33 s^{-1}.

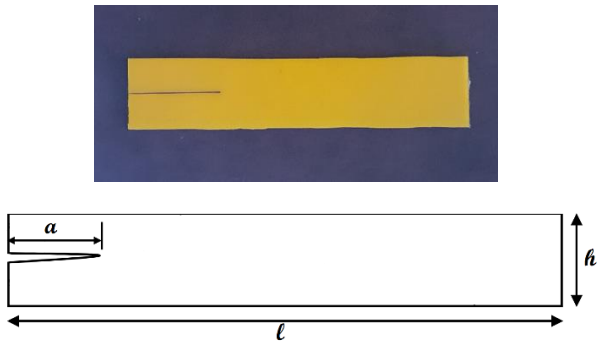

Specimen dimension	mm
Initial crack, a	35
Length, L	120
Width, w	20
Thickness	2.33

Fig.4. Tearing test specimens geometry and dimensions

Fig 5. Pure shear specimen subjected to the uniform strain rate in testing machine

The mode-I tearing energy is calculated as:

$$T = W_0 L_0 \tag{19}$$

Where, W_0 is the strain density function under pure shear region and L_0 is the height of the specimen between two rigid grips. The value of the strain density function, W_0, can be determined by integration under the load-displacement curve of pure shear specimen [19]. The obtained load-displacement curves for pure shear specimens with 3 different shore hardness are depicted in Fig. 6. The calculated critical tearing energies using (19) are listed in Table 2.

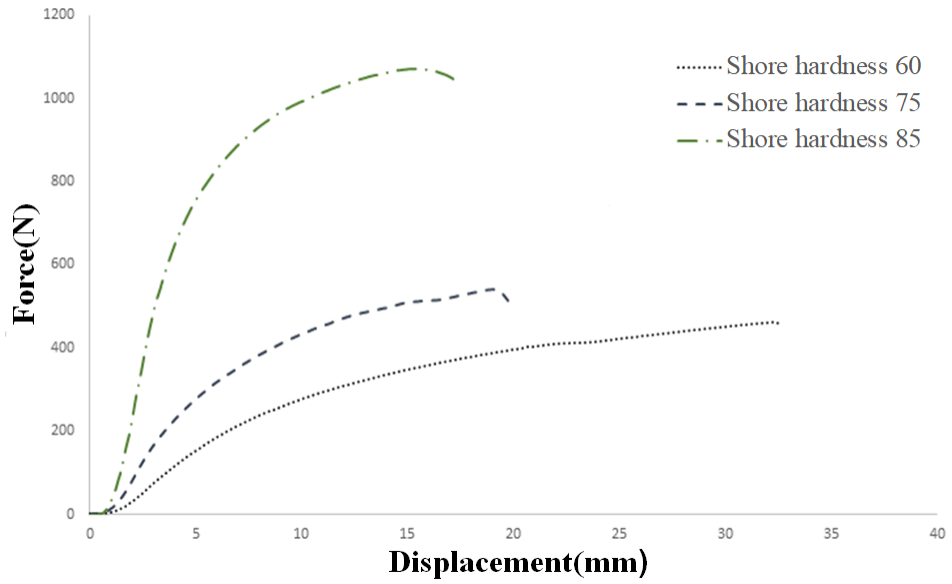

Fig 6. Load versus displacement for pure shear tearing specimens with 3 different shore hardness

Table 2. Calculated tearing energy for pure shear tearing specimens with different shore hardness

Shore hardness		**60**	**75**	**85**
Tearing energy (G)	KJ/m^2	4.180	5.941	6.989

3. Analyses and Results

A user material subroutine was developed to simulate the hyper viscoelastic and damage behavior in polyurethane elastomers. To investigate the hyper-viscoelastic damage evolution in polyurethane, the pure shear tearing specimen and the SENT specimen were simulated in Abaqus software linked to the developed user defined subroutine. To model the specimens, 3

dimensional 8 node elements (C3D8) were used in the finite element modeling. The developed subroutine verified by a single element subjected to the uniaxial tension loading under the strain rate of 0.33 /s. Fig.7 shows the element with dimension of 0.1 mm×0.1 mm×0.1mm and the boundary condition applied to it. The FEA result for 3 different shore hardness at strain rate of 0.33/s depicted in Fig.8 shows hyper viscoelastic behavior, damage initiation and damage evolution slopes.

Load	Displacement at y=0.1 mm
Boundary Condition	at x=0 ,U_1=0 at y=0, U_2=0 at z=0, U_3=0

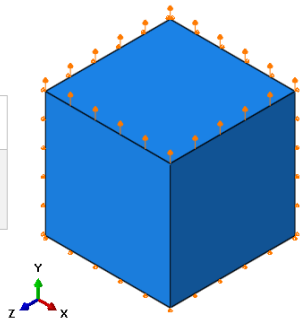

Fig7. Single element subjected to the uniaxial tension loading

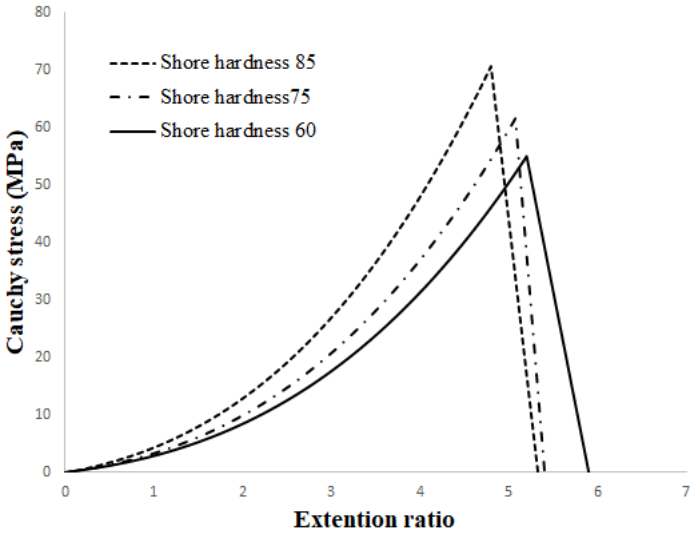

Fig8. FEA Single element results

3.1 SENT Model

A single edge notch tension (SENT) specimen which is a tensile strip of polyurethane material with a dimension of 40 mm×60 mm × 2.33 mm and an initial crack length of 12 mm, connected to rigid grips of the testing machine and subjected to a uniform strain rate of 0.33 s^{-1}. In FEA procedure, a quarter of the SENT specimen was modeled (half of width and thickness) to simulate the test with the same material properties and the geometry of the test specimens. The displacement-based loading with the strain rate of 0.33 s^{-1} was applied on the reference point located on the top surface of the model with the symmetry boundary conditions. Finite element analyses of the models were performed by Abaqus explicit solver linked with the developed user material subroutine. The deformation and tearing of the model with shore hardness of 85 during the time is shown in Fig. 10 comparing with the experimental results. Also is shown in the Figure, a close up view of the crack tip propagation with element deletion at the bottom layer. This figure shows a good agreement between the predicted response and the experimental images of the tensile strip test. In this analysis 1785 number of elements were employed. To ensure proper mesh size, an independent simulation using 2873 elements was conducted. Comparing obtained results from both simulations showed a less than 2% different in peak loads that considered mesh size is suitable for the analysis

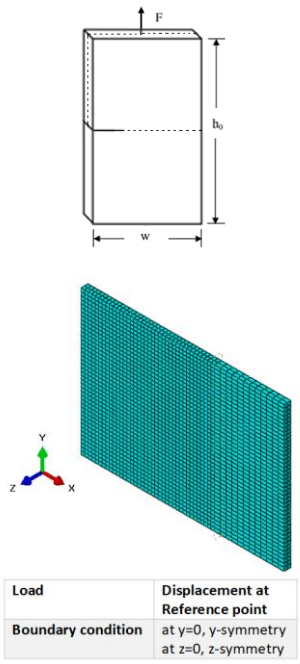

Fig.9 Geometry of the full specimen and FEM mesh for the quarter model of SENT specimen

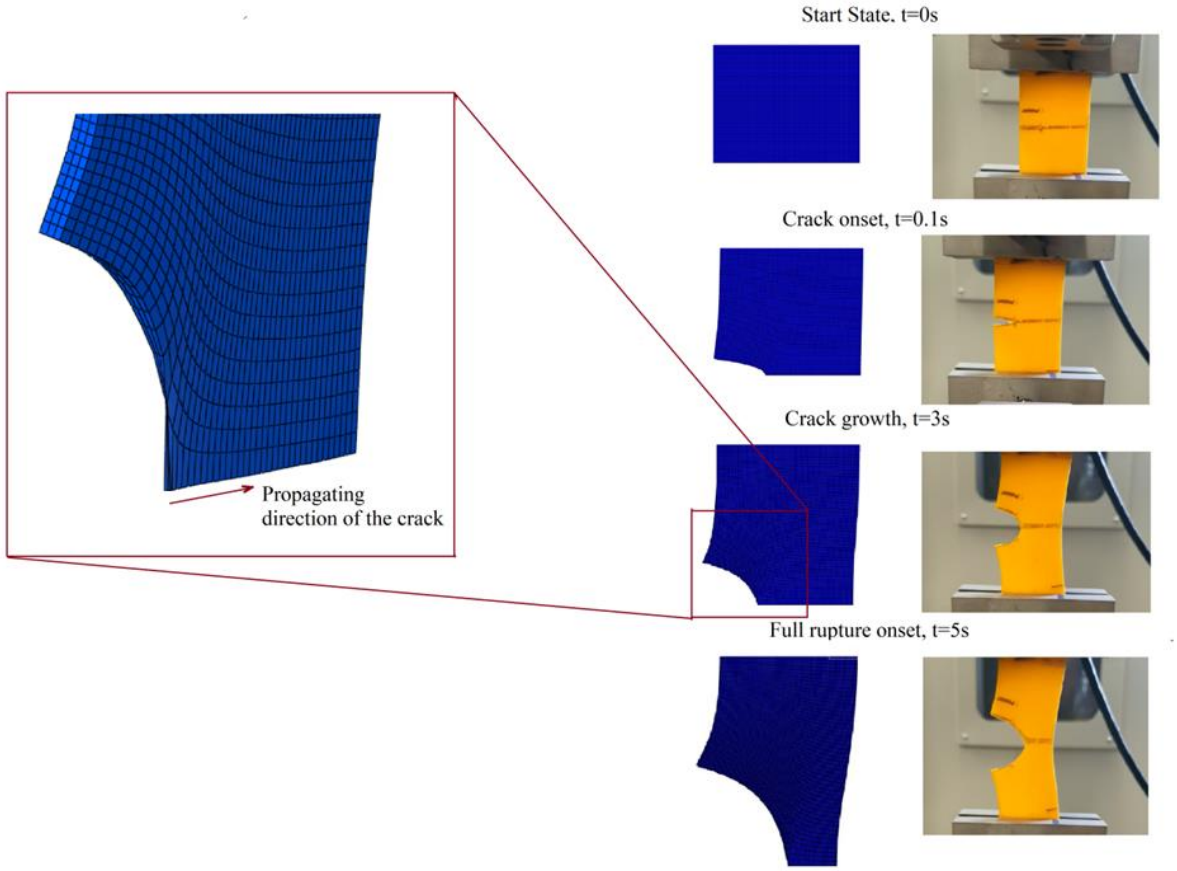

Fig. 10 Comparison of tearing in the experimental test and FEA modeling of Polyurethane with shore hardness of 85 under the strain rate of 0.33 s^{-1}

Two other tensile strip specimens with shore hardness of 60 and 75 are also analyzed by the finite element modeling and developed progressive damage analysis procedure. The obtained force-displacement histories for all three different shore hardness are compared with the experimental results and shown in Fig. 12.

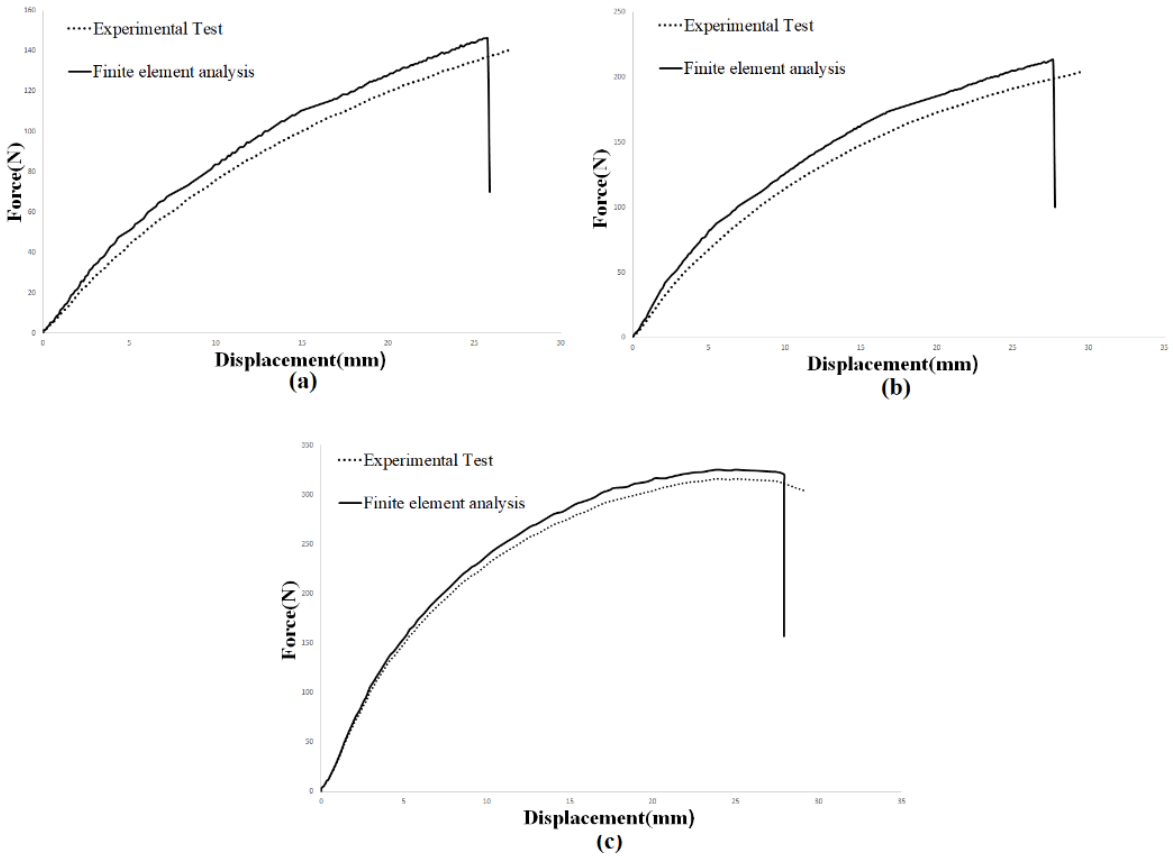

Fig. 12 Load-displacement curves of the SENT specimen for experimental test and FEA simulation under strain rate of 0.33 /s (a) shore hardness of 60, (b) shore hardness of 75, (c) shore hardness of 85

3.2 Pure Shear Tearing Model

To decrease the computational time and due to the existence of symmetry conditions, a quarter of the pure shear specimen (half of width and thickness) was modeled. The full specimen and the quarter model of that are shown in Fig.13. The dashed line in this figure shows the quarter model used in the FEA which has the symmetry boundary conditions. The displacement based loading with the strain rate of 0.33 s^{-1} was applied on the reference point located on the top surface of the model. The material properties and the geometry of the model are the same with the pure shear specimens of the experiments (Table.1 and Table.2). The developed user material subroutine based on the damage zone approach discussing in section 2, linked to the Abaqus explicit solver and used to analyze the damage initiation and evolution of the model. The deformation and tearing result of the FEA model with shore hardness of 75 is compared with the experimental

result in Fig.14 showing a good agreement between the predicted response and the experimental images of the pure shear tearing test. In this model also the crack tip propagated along with the element deletion at the bottom layer.

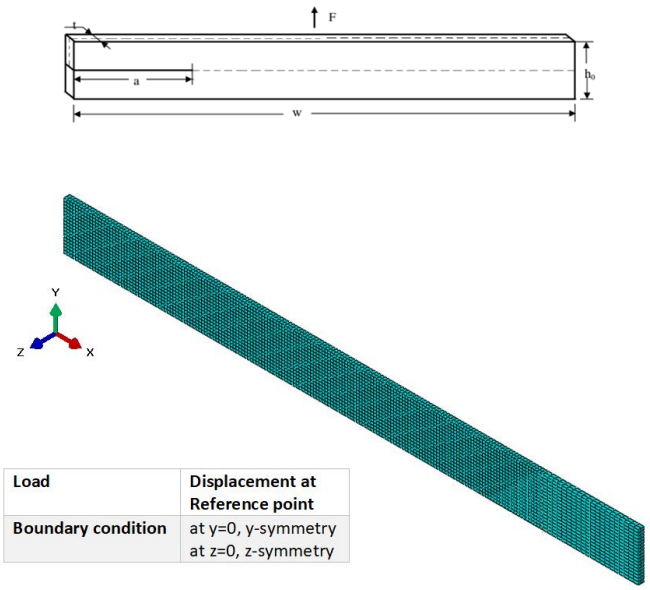

Fig. 13 Geometry of the full specimen and FEM mesh for quarter of the pure shear specimen

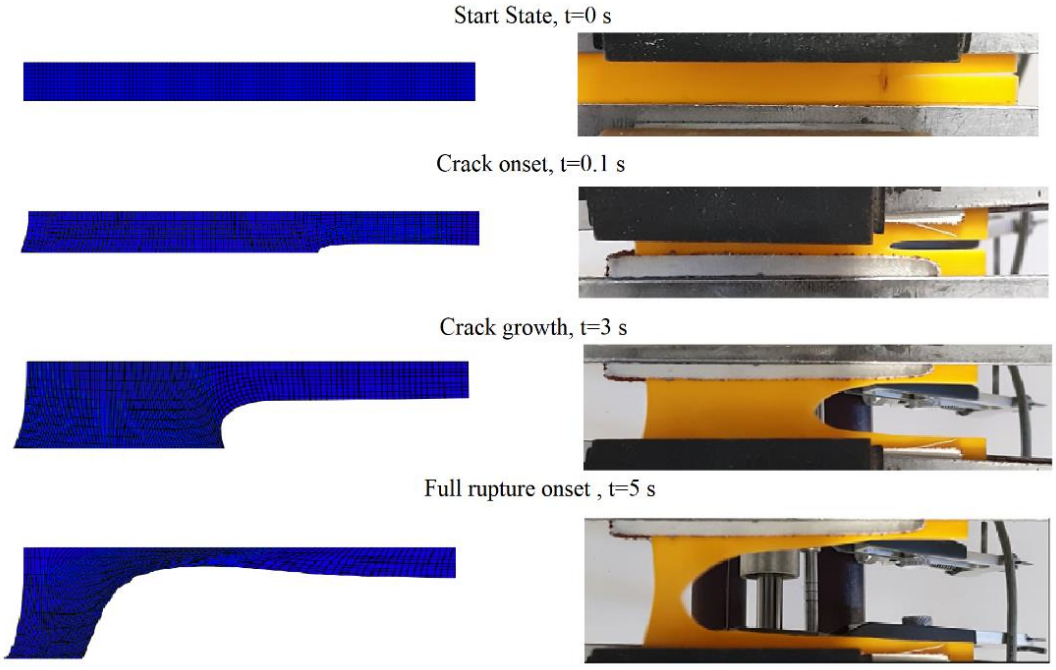

Fig. 14 Comparison of tearing in the experimental test and FEA modeling of Polyurethane with shore hardness of 75 under the strain rate of 0.33 s^{-1}

Two other pure shear specimens with shore hardness of 60 and 85 are also simulated in the FEA procedure. The force-displacement histories for all three different shore hardness are shown in Fig. 15. In this analysis 2530 number of elements were employed. To ensure proper mesh size, an independent simulation using 4123 elements was conducted. Comparing obtained results from both simulations showed a less than 2% different in peak loads that considered mesh size is suitable for the analysis.

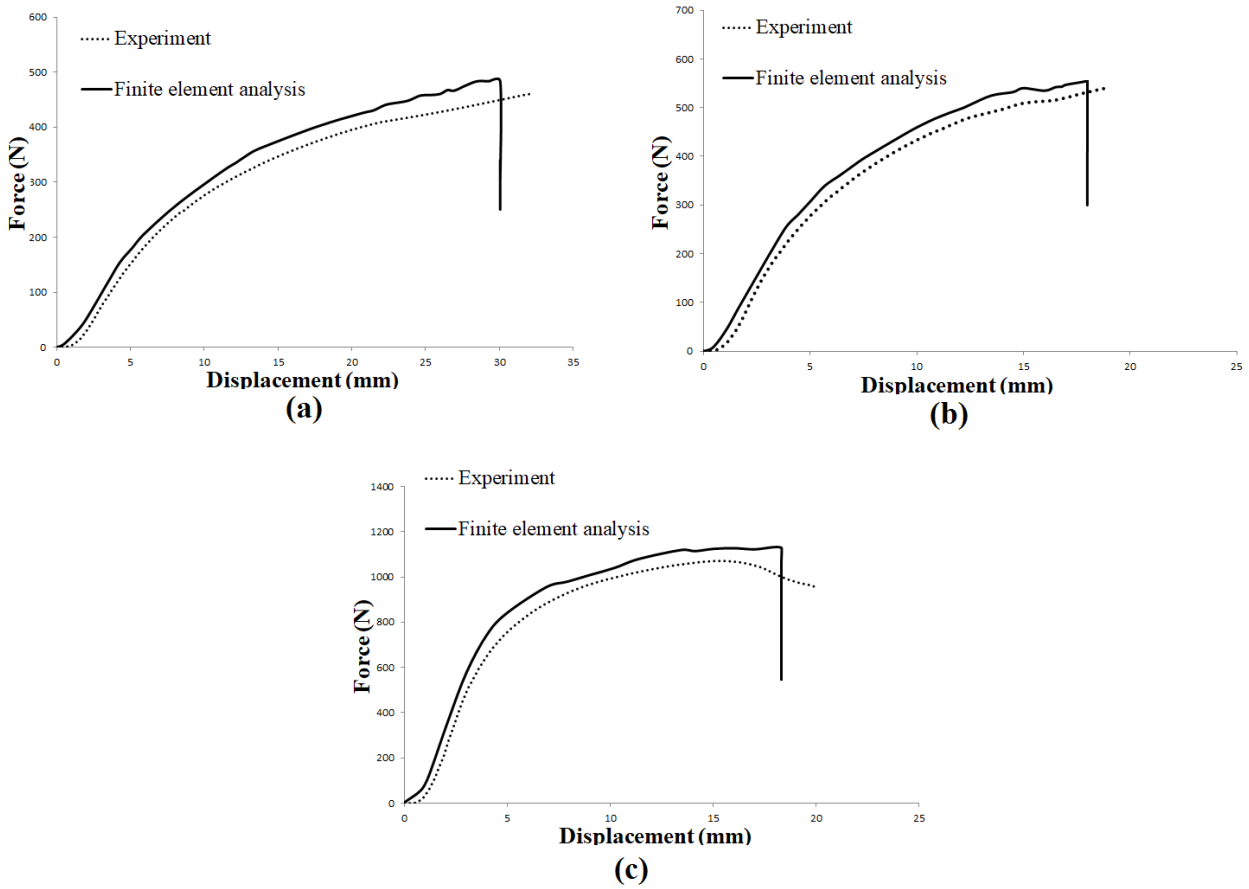

Fig. 15 Load-displacement curves for pure shear specimen from experiments and FEA simulations under strain rate of 0.33 s^{-1}, (a) shore hardness of 60, (b) shore hardness of 75, and (c) shore hardness of 85

Comparison between the FEA and experimental results shows that the trend of the force displacement curves for the experimental and FEA analysis before the beginning of tearing are very close together. The peak force at starting of tearing in all 3 different shore hardness is about 10-15% more than the peak force of the experimental results and the drop force of the FEA results occurs in smaller displacement values in comparison with the experimental results.

However, according to the highly nonlinear behavior of the material, it can be considered that there is a good agreement between the FEA and experimental results. As a result, it can be concluded that using the hyper viscoelastic strain density function in the damage zone modeling could be an effective methodology to predict the tearing of elastomeric materials.

Conclusion

A cohesive zone model based on the traction-separation law proposed by Li et al. was used to simulate the damage initiation and propagation of the elastomeric polyurethane materials. In the traction-separation diagram, the behavior of the elastomer before damage initiation is considered as hyper viscoelastic. In previous studies about the damage growth in elastomers, the hyper viscoelastic behavior was simulated using the rheological model which makes much complexity in numerical analysis. In this study, the simulation of the hyper viscoelastic behavior has been performed by implementing a rate-dependent factor proposed by Somarathna et al, to the Mooney-Rivlin function to make a more accurate prediction of the material behavior. The critical tearing energy used in the calculation procedure of the damage evolution has been determined by performing the tearing tests for all three shore hardness of the polyurethane elastomers. The material properties determined by the experimental tests were implemented in the FEA simulation procedure. In the present study, a developed user-defined material subroutine (VUMAT) linked to the FEA software was utilized to predict the damage evolution in pure shear specimens of the polyurethane material with 3 different shore hardness. A Comparison of the FEA simulation and experimental results showed that the damage zone approach based on the hyper viscoelastic strain density function can lead to good accuracy in the prediction of damage initiation and evolution in Polyurethane elastomers.

References

[1] Mei-Chen Lin1, Jia-Horng Lin, Limin Bao, “Thermoplastic Polyurethane Reinforced with Continuous Carbon Fiber Tows: Manufacturing Technique and Fabric Property Evaluation”, Journal of Applied Composite Materials, January 2021. https://doi.org/10.1007/s10443-021-09867-1

[2] Mark R. Gurvich, “Fracture Modelling and Characteriation of Elastomeric Materials and Composites for Design Application”, Rubber Chemistry and Technology, December 2010. https://doi.org/10.5254/1.3493425

[3] Arun U Nair, Hubert Lobo, and Anita M Bestelmeyer, “Characterization of Damage in Hyperelastic terials Using Standard Test Methods and Abaqus”, SIMULIA Customer Conference, 2009

[4] Elsiddig Elmukashfi1, Martin Kroon, “Numerical Modeling and Analysis of Dynamic Crack Propagation in Rubber”, 13th International Conference on Fracture June 16–21, 2013, Beijing, China

[5] Venkata Rama Lakshmi Preethi Bahadursha, “Tearing of Styrene Butadiene Rubber Using Finite Element Analysis”, Master Thesis, The Graduate Faculty of The University of Akron, 2015

[6] Yoav Lev, Konstantin Volokh,” Modeling Crack Propagation in Rubber”, 14th International LS-DYNA Conference, 2016

[7] K Volokh , “Review of the Energy Limiters Approach to Modeling Failure of Rubber”. Rubber Chemistry and Technology, American Chemical Society, 2013, 86, pp.470 - 487. ff10.5254/rct.13.87948ff. ffhal-01573585ff 10.5254/rct.13.87948

[8] Adel Hamdi, Sofiane Guessasma, M. Naït Abdelaziz, “Fracture of Elastomers by Cavitation”, Materials and Design 53 (2014) 497–503 https://doi.org/10.1016/j.matdes.2013.06.058

[9] Bo Li, Venkata Rama Lakshmi Preethi Bahadursha, Michelle S. Hoo Fatt, “Predicting Failure in Rubber Membranes: An Experimental-Numerical Approach”, Engineering Failure Analysis 90 (2018) 404–424. https://doi.org/10.1016/j.engfailanal.2018.04.003

[10] Griffith, A. A., ‘‘The Theory of Rupture,’’ in Biezeno, C. B., and Burgers, J. M. (eds.), The Proceeding of the First International Congress for Applied Mechanics, Delft, the Netherlands, 1925, pp. 55–63. doi: 10.12691/ajme-5-3-4.

[11] Rivlin, R. S. and Thomas, A. G., ‘‘Rupture of Rubber. I. Characteristic Energy for Tearing,’’ Journal of Polymer Science, Vol. 10, 1953, pp. 291–318. https://doi.org/10.1002/pol.1953.120100303

[12] H.M.C.C. Somarathna, S.N. Raman, D. Mohotti, A.A. Mutalib, K.H. Badri,” Hyper-viscoelastic Constitutive Models for Predicting the Material Behavior of Polyurethane under Varying Strain Rates and Uniaxial Tensile Loading”, Construction and Building Materials 236 (2020) 117417. https://doi.org/10.1016/j.conbuildmat.2019.117417

[13] Standard Test Methods for Vulcanized Rubber and Thermoplastic Elastomers— Tension, ASTM D-412

[14] M.Jahanmardi, H.Hosseini Toudeshky, MS.Goodarzi, “Experimental Hyper-viscoelastic Constitutive Model for Numerical Study of Elastomer Materials”, Applied Nanoscience Journal, July 2022 https://doi.org/10.1007/s13204-022-02554-y

[15] Thomas, A.G., “The Development of Fracture Mechanics for Elastomers,” Goodyear Medal Paper presented to the American Society Rubber Division Meeting Chicago, April 1994,

Rubber Chemistry and Technology, Vol. 67, No. 3, G50-G60, 1994. https://doi.org/10.5254/1.3538688

[16] Lake, G.J., "Fatigue and Fracture of Elastomers," Rubber Chemistry and Technology, Vol. 68, No. 3, pp. 435-460, 1995. https://doi.org/10.5254/1.3538750

[17] Lake, G.J., Lawrence, C.C. and Thomas, A.G., "High-Speed Fracture of Elastomers: Part I," Rubber Chemistry and Technology, Vol. 73, No. 5, pp. 801-817, 2000. doi: 10.3390/ma14030601

[18] Lake, G.J. and Thomas, A.G., "Strength," in Engineering with rubber, How to design rubber components, 2nd edition, A.N. Gent (editor), Hanser Gardner Publications, Cincinnati, 2001.

[19] Lake, G.J., "Fracture Mechanics and its Application to Failure in Rubber Articles," Rubber Chemistry and Technology, Vol. 76, No. 3, pp.567-591, 2003. https://doi.org/10.5254/1.3547761